Human-Robot Interaction Tests on a Novel Robot for Gait Assistance

Nevio Luigi Tagliamonte, Fabrizio Sergi, Giorgio Carpino, Dino Accoto and Eugenio Guglielmelli

***Abstract*—This paper presents tests on a treadmill-based non-anthropomorphic wearable robot assisting hip and knee flexion/extension movements using compliant actuation. Validation experiments were performed on the actuators and on the robot, with specific focus on the evaluation of intrinsic backdrivability and of assistance capability. Tests on a young healthy subject were conducted. In the case of robot completely unpowered, maximum backdriving torques were found to be in the order of 10 N m due to the robot design features (reduced swinging masses; low intrinsic mechanical impedance and high-efficiency reduction gears for the actuators). Assistance tests demonstrated that the robot can deliver torques attracting the subject towards a predicted kinematic status.**

I. Introduction

Wearable Robots (WRs) are actuated systems used to complement or substitute motor functions, operating alongside limbs (active orthoses) or replacing missing limbs (robotic prostheses) [1]. During the last years, several review papers and books on wearable robotics, in particular on lower-limbs systems (e.g. [2], [3], [4]), have been published, proving the high interest of the scientific community in this research area. Autonomous active orthoses are commonly designed to assist disabled subjects in daily life scenarios. Some examples of portable systems are the Ekso (developed by Ekso Bionics, Berkeley, USA) [5], the ReWalk (developed by Argo Medical Technologies, Yokneam Illit, Israel) [6], the REX (developed by REX Bionics, Auckland, New Zealand) [7], the HAL-5 (developed by Cyberdyne, Tsukuba, Japan) [8], the Vanderbilt powered orthosis [9], and the Mina [10]. Treadmill-based active orthoses are used for rehabilitation purposes and also typically include body-weight support systems. Representative systems are the Lokomat (developed by Hocoma, Volketswil, Switzerland) [11], the LOPES (LOwer-extremity Powered ExoSkeleton) [12], the AutoAmbulator [13], the ALEX (Active Leg EXoskeleton) [14], the PAM-POGO (Pelvic Assist Manipulator - Pneumatically Operated Gait Orthosis) [15]. Current research is also moving towards the inclusion of compliant elements [16] or variable impedance actuators [17], [18].

All the mentioned robots have a kinematic structure which is essentially anthropomorphic, i.e. it replicates the features of the musculoskeletal system because of the direct correspondence between robotic and human joints and between robotic links and human segments. In such robots, kinematic incompatibilities can arise from the imperfect alignment with human joint axes of rotation. In particular, macro- and micro-misalignments [19] can cause the exchange of unwanted interaction forces (e.g. reaction forces on the articulations or shear forces on the skin), resulting in discomfort and even pain for the user [20]. Conversely, non-anthropomorphic structures are intrinsically robust against misalignments, thus allowing improved ergonomics and kinematic compatibility. Moreover, the increased design freedom provided by the larger number of design parameters opens the opportunity of optimizing the dynamical properties and/or the actuation system.

The Authors have recently developed a non-anthropomorphic treadmill-based robot that assists hip and knee motion in the sagittal plane using compliant actuators. Robot design is based on previous works describing a novel approach to kinematic synthesis, selection and morphological optimization: a systematic search of all admissible (i.e. kinematically compatible) planar 2-DOFs solutions [21] and an optimization process minimizing static torques demanded to the actuators [22]. Moreover, actuators have been designed to have low intrinsic impedance and accurate torque control.

This paper presents experimental results on the validation of some relevant aspects of physical human-robot interaction, such as robot backdrivability and assistance capability. Experimental tests were performed on a healthy young subject to demonstrate that the robot can be easily backdriven also when the actuators are unpowered, and that kinematic patterns remain close to physiological ones. Moreover, the possibility of supporting gait is demonstrated, employing a control scheme which adapts to the natural walking pattern of the subject.

II. Robot Prototype

A. Mechanical structure

The robot, depicted in Fig. 1(a), is composed (for each leg) of: *i)* Supporting links, whose kinematics have been designed on the basis of the optimization process described in [22]. *ii)* Two rotary Series Elastic Actuators (SEAs) actuating joints A and D; *iii)* One cuff at the pelvis level (joint A), one cuff at the thigh level (joint B) and one cuff at the shank level (joint C). The segment EF can be manually adjusted to adapt robot kinematic structure to users between the 5$^{\text{th}}$ and the 95$^{\text{th}}$ percentile of adult population. Other regulations are allowed by sliders: position of the joints A, B and C on the pelvis cuff, the thigh cuff and the shank cuff respectively. To achieve a compact design and to reduce swinging masses connected to distal portions of the legs, the actuators are arranged close to the trunk as shown in Fig. 1(a).

B. Actuation system

The design architecture of the developed SEA has been conceived to shift the actuator center of mass with respect

This work was conducted when all the Authors were with Università Campus Bio-Medico di Roma, Laboratory of Biomedical Robotics and Biomicrosystems, Center of Integrated Research (CIR), Via Álvaro del Portillo, 21 - 00128 Rome, Italy. F. Sergi is now with Rice University, MEMS Department, Houston, TX 77005, USA.

Corresponding author: n.tagliamonte@unicampus.it

978-1-4673-6024-1/13/$31.00 ©2013 IEEE

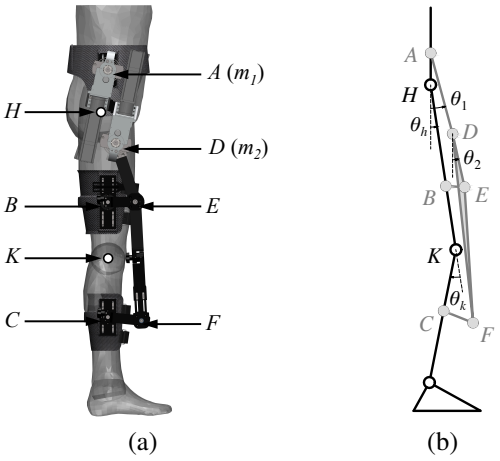

(a) (b)

Fig. 1. (a) Structure of the robot. Blank circles, points H and K, represent the human hip and knee joints respectively. Points A and D are the actuated robotic joints, also indicated as m_1 and m_2. (b) Schematic representation of the human (black) and robot (gray) kinematic structures. Robot actuated joint angles θ_1 and θ_2 and human joint angles θ_h (hip) and θ_k (knee) are highlighted. Actuator rotation angles (counterclockwise motion is positive) can be calculated as $\theta_{m_1} = \theta_1$ and $\theta_{m_2} = \theta_2 - \theta_1$.

to the actuated joint (i.e. the gearmotor is placed alongside human limbs). In each SEA, a Maxon EC-4pole brushless DC motor (rated power: 300 W) is connected to the output shaft through a compact monolithic disc-shaped torsional spring. Its design is based on an iterative FEM (Finite Element Method) simulation-based design and optimization process [23], to get a target stiffness of 250 N m/rad. A two stage reduction gear (overall reduction ratio: 64.5:1, theoretical efficiency: 76.5%) is placed between the motor and the elastic element. Spring deflection is measured using two Gurley A10 absolute encoders (resolution: 15 bits). The actuators can provide a maximum continuous torque of 30 N m and a peak torque of about 60 N m.

C. Treadmill-based platform

The treadmill-based platform is shown in Fig. 2. The treadmill is the N-Mill from ForceLink B.V.. It has a walking surface of 70×175 cm, a walking speed in the range 0.1–12 km/h, adjustable sidebars and a frame to connect a safety harness for fall prevention. The robot is suspended to a support system able to dynamically and passively compensate its weight (about 25 kg). The system is able to generate a constant vertical force, it is dimensioned not to introduce resonance at natural walking frequencies and to minimize inertia perceived by the user. It also has adjustable height to adapt to the anthropometric measurements of different subjects. Cables are used to connect the weight balancing system to the pelvis cuff thus allowing unconstrained torso rotations.

III. Robot Control

A. Control architecture

Each of the four SEAs of the robot is torque-controlled. Torque regulation is based on the measurement of the spring deflection, i.e. the difference between the SEA output rotation and the gearmotor rotation. The control scheme used in this work is based on the cascaded approach proposed in [24].

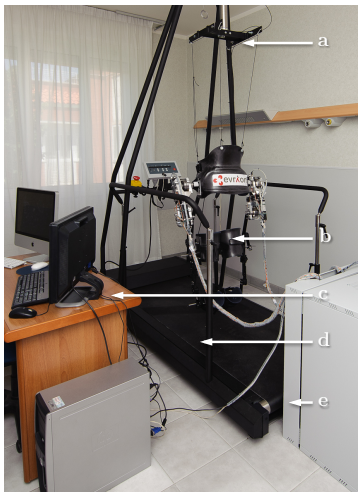

Fig. 2. Treadmill-based platform. a: Robot weight support system; b: Wearable robot; c: Control station; d: Treadmill; e: Electronic rack.

It consists of a PI velocity control loop nested in a PI torque control loop. The robot is stiffness-controlled in the joint space, i.e. the desired torque for each actuated joint (right leg r and left leg l) is set as:

$$\tau_{m_i,d}(t) = -k_{m_i}[\theta_{m_i}(t) - \theta_{m_i,d}(t)] \quad (1)$$

being θ_{m_i} and $\theta_{m_i,d}$ the actual and the desired actuator rotations respectively, and k_{m_i} the virtual stiffness ($i = 1, 2$).

B. Control hardware

The control hardware consists of: *i)* Four Maxon EPOS2 70/10 control units to drive SEA brushless DC motors, connected to two Maxon Shunt Regulators DSR 70/30 limiting supply voltage increases. *ii)* A National Instruments compactRIO-9022 unit (cRIO), with a reconfigurable Field-Programmable Gate Array (FPGA) module and an embedded controller running LabVIEW Real Time (RT) software. The cRIO also comprises a high-speed digital I/O module to acquire the signals from the absolute encoders, and a high-speed CAN module (1 Mbit/s) for communication with the EPOS2 units. The FPGA module of the cRIO system is programmed to acquire SEA absolute encoder signals (SSI communication) and to execute CAN bus low-level communication with the EPOS2 controllers (transmission of motor commands and reading of current, position and velocity). Torque controllers run on the RT level (250 Hz) of the cRIO device and they generate desired velocity commands that are transmitted via CANopen protocol to the velocity controllers running on the EPOS2 devices (1 kHz). EPOS2 units, shunt regulators, cRIO device, and power supplies are supported by a remote electronic rack.

C. AFO-based control

Assistive torques are provided following the approach proposed in [25] and briefly summarized here. The control method is based on a pool of K Adaptive Frequency Oscillators (AFOs), which learn periodic joint angles $\theta(t)$ in steady-state conditions. The differential equations of the phase $\phi_j(t)$

and the frequency ω_j(t) of the j-th AFO ($j \in [0, K-1]$), implemented using a phase oscillator, are:

$$\begin{cases} \dot{\phi}_j(t) = j\omega(t) + \nu F(t)\cos\phi_j(t) \\ \dot{\omega}(t) = \nu F(t)\cos\phi_1(t) \\ \dot{\alpha}_j(t) = \eta F(t)\sin\phi_j(t) \end{cases} \quad (2)$$

The frequency converges, with a convergence constant ν, to one of the frequencies of the input teaching signal $F(t) = \theta(t) - \hat{\theta}(t)$, with $\hat{\theta}(t) = \sum_{j=0}^{K-1} \alpha_j \sin\phi_j(t)$. In particular, only the fundamental frequency is learned, the others being multiples of it. In addition, the oscillators are coupled to a non-linear filter, a sum of weighted Gaussian-like kernels as a function of the phase $\phi_1(t)$. An iterative local regression continuously learns the weights to estimate joint angle $\hat{\theta}^*(t)$. Therefore, the angle at a time corresponding to a Δ_ϕ phase lead in the future, indicated as $\hat{\theta}^{*,\Delta_\phi}(t)$, is derived. For each joint the assistive torque is then calculated as in (1), by setting $\theta_{mi}(t) = \hat{\theta}^{*,\Delta_\phi}_{m_i}(t)$. With this approach, the user is attracted towards her/his estimated future kinematic status by elastic torques, with the opportunity to continuously adapt the frequency and the amplitude/shape of the attractive pattern. Moreover, this approach allows not to necessarily rely on forward/inverse kinematics to produce assistive torques.

IV. Experimental Tests

A. Tests on the actuators

1) Bench tests: Experimental tests were performed to assess torque tracking capability of the developed SEAs. To this aim a custom dynamometric test-bed was used. As a first step the torque-deflection characteristic for the springs were evaluated. Each SEA output shaft was connected to a torque sensor to measure the torque delivered to statically generate imposed deflections (measured by absolute encoders) in loading and unloading directions. Therefore, torque and deflection data were fitted, finding high linearity for all the springs and an average stiffness of 270.2 ± 3.1 N m/rad. This value differs only 14.6% from the one targeted in FEM simulations. The discrepancy is even lower than the one achieved by the Authors in previous works on the design of torsional elements for SEAs [23]. Torque control regulation was evaluated by connecting the output shaft of the SEA to the frame, i.e. considering the deflection of the elastic element without any external disturbance. The transfer function between desired and actual torques was determined by using a non parametric identification method [26]. The desired torque was set to be a Schroeder multisine waveform with a flat spectrum in the range $0.1-10$ Hz (negligible power content above 10 Hz) and a peak value of 15 N m (half of the nominal torque of the actuator). A quite flat transfer function was found, with an amplitude attenuation of 3 dB at about 6.5 Hz.

2) Robot tests: To estimate the order of magnitude of the torques needed to actuate the robot in free space, physiological walking movements were produced with the robot not worn and the actuators stiffness-controlled as described in (1). Desired actuator kinematic profiles were calculated starting from physiological walking datasets [27], and using the inverse kinematics solving routine derived in [22]. Virtual stiffness was set to $k_{mil} = k_{mir} = 1$ N m/deg (57.3 N m/rad) for $i = 1, 2$. Results demonstrate the capability of the system of producing suitable walking patterns with peak torques lower than 7 N m (12% of the maximum value allowed by the actuators). Since this test was performed at slow walking speed, torques delivered to actuate the robot were needed to compensate mainly gravitational and frictional effects. Therefore, 88% of the actuator deliverable torques (i.e. 53 N m) is still available to provide physical assistance during walking.

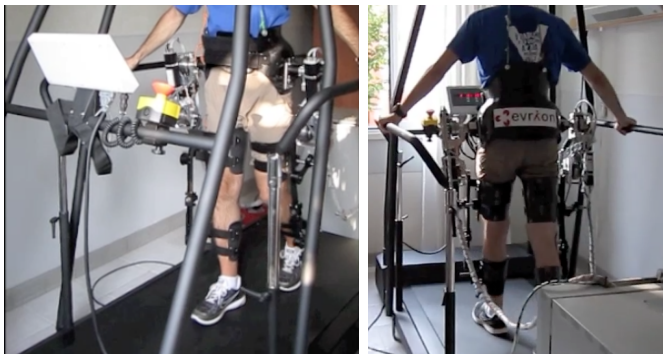

(a) (b)

Fig. 3. Front (a) and back (b) views of the robot worn by a tester.

B. Tests on a human subject

A voluntary healthy man (28 years old, height 180 cm, body mass 80 kg) was asked to walk on the treadmill wearing the robot. Cuffs were fastened to the pelvis, the thighs and the shanks, assuring that they could not significantly move during the trials and they could be comfortable enough for the subject. For safety reasons, a push button able to interrupt power supply of the treadmill and of the robot actuators was accessible to the tester during the trials. Before the tests, the subject was asked to freely walk at a self-selected walking speed for 10 minutes (robot unpowered) to get familiar with the device and with the testing environment. Pictures of the subject wearing the robot are reported in Fig. 3. Before each test, actuator encoders and measured spring deflections were initialized to the straight leg configuration while the subject was not moving for 5 s.

1) Robot wearing procedure: When the user accesses the platform he wears the pelvis cuff and the robot suspension height is regulated by manually acting on the weight balancing system. Therefore, velcro straps on the pelvis cuff (anterior closing system and shoulder straps) are fastened. Subsequently, the thigh and shank cuffs are worn and fastened. Adjustable links and sliders on the cuffs (see section II-A) are regulated to allow links BE and CF (see Fig. 1) to be almost perpendicular to the human segments. Anthropometric measures of the selected tester (thigh and shank segments) and adjusted robot dimensions are reported in Tab. I. Before tests start the subject is asked to perform simple hip and knee flexion/extension movements to assess the perceived comfort.

2) Backdrivability tests: These tests aim at evaluating robot intrinsic transparency, i.e. at verifying that a human subject can walk in a physiological way also when the robot is unpowered. For this test, actuators are switched off and the user has to backdrive the robot at different walking speeds (2.0, 2.5 and

TABLE I. LENGTH OF ADJUSTED ROBOTIC LINKS AND OF TESTER'S BODY SEGMENTS.

Link/segment	AH	HB	KC	EF	Thigh	Shank
Length [mm]	120	300	230	355	460	440

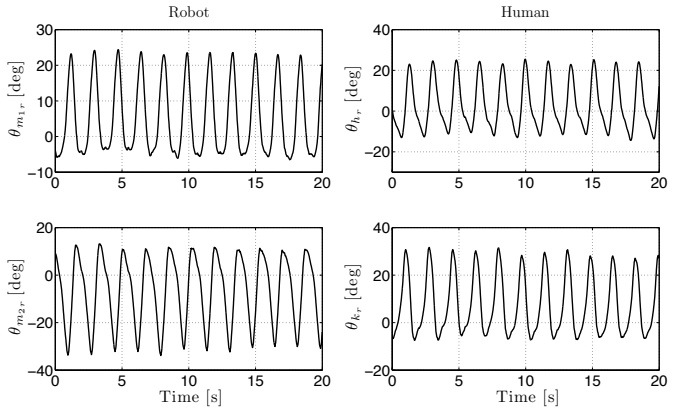

Fig. 4. Robot actuator and human joint rotations for the backdrivability test performed at a walking speed of 2.5 km/h. Representative data for the right leg, in steady-state conditions, are reported. Gait cycle (calculated as the average over 10 periods) is 1.71 s.

3.0 km/h). In these conditions, the actuated joint rotations ($\theta_{m_{ir}}$ and $\theta_{m_{il}}$, $i = 1, 2$) and human-robot interaction torques in the robot joint space ($\tau_{m_{ir}}$ and $\tau_{m_{il}}$, $i = 1, 2$) are recorded. The transformation from the robot joint space to the human joint space, for each leg, is calculated as in [22], to obtain angles (θ_h, θ_k) and torques (τ_h, τ_k) of the hip and knee joints. The conventions for the rotations are reported in Fig. 1(b). Robot actuator and human joint angles of the right leg are reported in Fig. 4, for a representative test at a walking speed of 2.5 km/h. The Gait Cycle (GC) for this test (calculated averaging over 10 periods) is 1.71 s. Interaction torques for the same test, average and standard deviation calculated over 10 cycles, are reported in Fig. 5 (robot joint domain) and in Fig. 6 (human joint domain). RMS and peak torque values are reported in Tab. II, comparing results of tests at different walking speeds. In the worst case (actuator m_{2l}), peak torques at the robotic joints level are 9.1 N m, 9.9 N m and 12.5 N m for the three selected velocities. The peak backdriving torques for the four actuators are 6.8 ± 1.6 N m, 8.9 ± 1.5 N m and 11.0 ± 1.4 N m for the three cases. In the human joint domain, peak backdriving torques in the worst case are 10.5 N m, 12.1 N m and 13.9 N m for the three selected speeds. The peak backdriving torques for the four human joints are 6.2 ± 3.0 N m, 8.8 ± 3.5 N m and 9.3 ± 4.0 N m for the three testing velocities. This result demonstrates the intrinsic backdrivability of the robot, due to the reduced mass and inertia of the structure and to the low impedance of the actuators. With unpowered actuators, a subject has to deliver low additional torques in order to backdrive the robot, i.e. around 15–20% of those required during free overground walking.

3) Assistance tests: Torque delivered for gait assistance are generated according to the control scheme described in section III-C. During assistance tests, the subject is initially asked to walk freely at a selected walking speed (2.5 km/h) with actuators switched off. In this phase, AFOs learn kine-

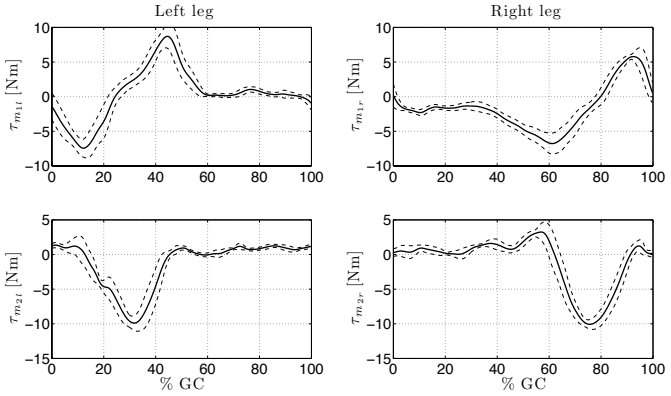

Fig. 5. Human-robot interaction torques in the robot joint space (as a function of the percentage of the gait cycle) for the backdrivability test performed at a walking speed of 2.5 km/h. Steady-state conditions are reported. Data are averaged over 10 gait cycles. Solid line: mean value; dashed lines: standard deviation.

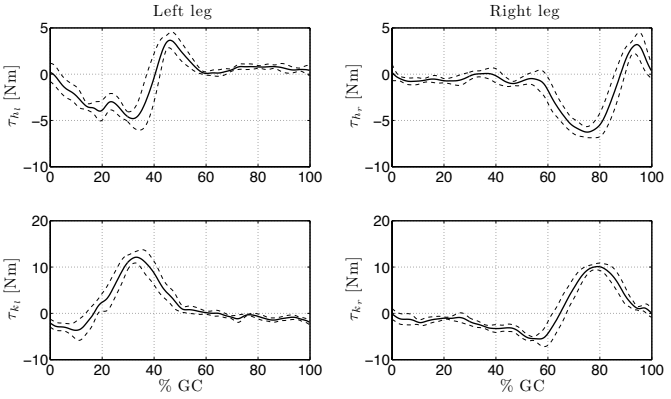

Fig. 6. Human-robot interaction torques in the human joint space (as a function of the percentage of the gait cycle) for the backdrivability test performed at a walking speed of 2.5 km/h. Steady-state conditions are reported. Data are averaged over 10 gait cycles. Solid line: mean value; dashed lines: standard deviation.

TABLE II. RMS AND PEAK VALUES FOR THE INTERACTION TORQUES (IN THE ROBOT AND HUMAN JOINT SPACES) DURING BACKDRIVABILITY TESTS AT DIFFERENT WALKING SPEEDS. VALUES ARE AVERAGED OVER 10 GAIT CYCLES.

Torque [Nm]	Walking speed [km/h]		
(Robot space)	2.0	2.5	3.0
$\tau_{m_{1l}}^{RMS}$	2.4	3.8	4.0
$\tau_{m_{1l}}^{peak}$	6.4	8.7	11.0
$\tau_{m_{2l}}^{RMS}$	3.3	3.7	4.6
$\tau_{m_{2l}}^{peak}$	9.1	9.9	12.5
$\tau_{m_{1r}}^{RMS}$	2.5	3.6	4.1
$\tau_{m_{1r}}^{peak}$	5.8	6.8	9.1
$\tau_{m_{2r}}^{RMS}$	2.8	4.0	4.3
$\tau_{m_{2r}}^{peak}$	5.7	10.1	11.0

Torque [Nm]	Walking speed [km/h]		
(Human space)	2.0	2.5	3.0
$\tau_{h_l}^{RMS}$	1.7	2.3	2.7
$\tau_{h_l}^{peak}$	4.6	4.8	6.1
$\tau_{k_l}^{RMS}$	4.0	4.7	5.4
$\tau_{k_l}^{peak}$	10.5	12.1	13.9
$\tau_{h_r}^{RMS}$	1.7	3.0	2.7
$\tau_{h_r}^{peak}$	3.8	7.0	6.0
$\tau_{k_r}^{RMS}$	3.5	5.0	5.0
$\tau_{k_r}^{peak}$	5.7	11.2	11.3

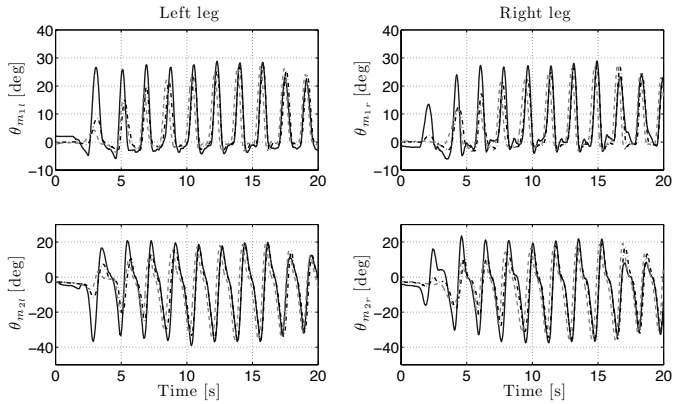

Fig. 7. AFO-based kinematic estimation in the robot joint space with actuators switched off during a test at 2.5 km/h walking speed. Solid line: measured angle θ_{mi}; Dashed black line: estimated angle $\hat{\theta}^{*}_{m_i}$; Dashed gray line: predicted (shifted) angle $\hat{\theta}^{*,\Delta_\phi}_{m_i}$. The shift Δ_ϕ is 10% of the gait cycle.

matics in the robot joint space $\hat{\theta}^{*}_{m_i}$ and continuously calculate it with a phase lead in the future $\hat{\theta}^{*,\Delta\phi}_{m_i}$. A representative graph of AFO-based kinematic prediction is reported in Fig. 7. The shift Δ_ϕ is set to 10% of the gait cycle. It can be observed that estimated kinematic profiles only require few gait cycles to converge to the real ones, and that the predicted kinematic status can be used as desired equilibrium position towards which the subject can be attracted. The torques delivered by the four actuators during a representative assistance test are depicted in Fig. 8. At $t = \bar{t} = 24.5$ s assistance is enabled and virtual stiffness is set to $k_{m_{il}} = k_{m_{ir}} = k_v$ $(i = 1, 2)$. Therefore, its value is manually changed as reported in the lower graph of Fig. 8. Modifying virtual elasticity corresponds to changing assistance level since the robot displays a more or less compliant behavior. Profiles reported in unassisted mode (gray band in Fig. 8) are interaction torques due to the action of the subject, who has to backdrive the robot (powered off). The decreasing of the torques for 24.5 s $< t <$ 43 s is due to the small magnitude of the desired torques caused by the low value of the set virtual stiffness. This corresponds, with reasonable approximation, to set to zero the desired torques, so that transparency of the robot is slightly increased. For $t > 43$ s significant assistance torques are delivered, increasing with k_v. In Fig. 8 the relationship between the assistive torques and the virtual stiffness is not linear as expected. This is likely caused by a slight modification of the human joint kinematic patterns, due to the tester's adaptation to the action of the robot.

For the same test, a representative example of actuators torque tracking capability is reported in Fig. 9 (actuator m_{1r}). For $t < \bar{t}$, backdriving torque is represented. Torque tracking is obtained within a maximum error of 3.5 N m with best performances in the high-stiffness range ($k_v > 0.25\, k_s$). A detail of torque tracking for 55 s $< t <$ 75 s is highlighted, showing a maximum error of 2 N m. Reduced tracking fidelity for low torque values is in agreement with previous characterization studies [28], showing that the selected linear control scheme has transparency limitations since it does not fully compensate for actuator friction.

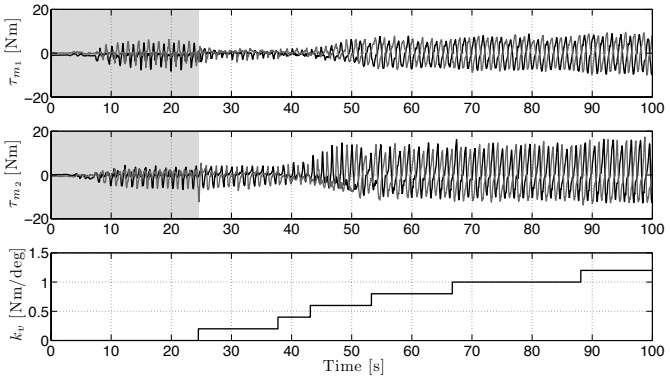

Fig. 8. Actuator torques τ_{m_1} and τ_{m_2} delivered during a representative assistance test. Black line: right leg; Gray line: left leg; Gray band: unassisted mode (actuators powered off). At $t = \bar{t} = 24.5$ s assistance is enabled. Virtual stiffness in control law (1) is $k_{m_{il}} = k_{m_{ir}} = k_v$ $(i = 1, 2)$ and is manually changed as reported in the lower graph.

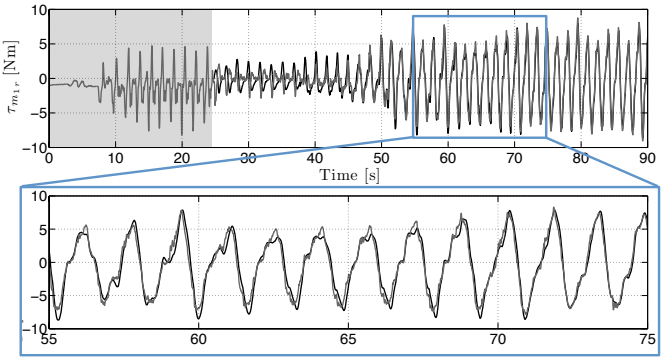

Fig. 9. Representative example of torque tracking capability during an assistance test (actuator m_{1r}). Black line: desired torque; Gray line: actual torque; Gray band: unassisted mode (at $t = \bar{t}$ assistance is enabled). Torque measured for $t < \bar{t}$ is due the action of the user, who backdrives the robot. Increasing torques for $t \geqslant \bar{t}$ are due to an increasing level of assistance (see Fig. 8). A detail of torque tracking for 55 s $< t <$ 75 s is highlighted.

V. Conclusions and Future Work

The paper presents preliminary tests on a novel non-anthropomorphic wearable robot including compliant actuators (SEAs) and assisting hip and knee motion in the sagittal plane (flexion/extension).

Validation experiments were carried out on the SEAs and on the robot, the latter being focused on assessing intrinsic backdrivability and assistance capability. The torque-angle characteristics for the SEA springs were derived correlating imposed deflections and measured torques. Torque control bandwidth of the actuators was identified: a rather flat transfer function with an attenuation of 3 dB at 6.5 Hz was found. The achieved bandwidth is suitable for accurate and high-fidelity torque tracking in walking assistance applications. The actuators were stiffness-controlled when mounted on the robot and commanded to track kinematic patterns producing physiological walking motion in free space. This experiment demonstrated that only 12% of peak torques deliverable by the actuators is needed to move the robot structure (mainly to compensate for gravity and friction effects) while the remaining 88% is available to provide physical assistance.

Tests with a young healthy subject were conducted to verify robot intrinsic transparency at different walking speeds. With the robot unpowered, backdriving torques were found to be in the order of 10 N m (15–20% of torques delivered by human joints during free overground walking) thus demonstrating the high backdrivability of the system. This result is due to the location of swinging masses in proximal districts, and to the intrinsic low mechanical impedance of the actuated joints, the latter being allowed by the presence of elastic components, the high efficiency in the transmission stages and the reduced friction in rotating parts. Assistance tests demonstrated that the robot can provide torques using AFO-based control approach. An increasing level of assistance was set by manually changing the value of the virtual stiffness in the assistive elastic torques. Starting from the the case of disabled actuators, interaction torques initially reduced for low values of the virtual stiffness, then they increased producing the requested assistance. During human-robot interaction tests no particular pain, discomfort or fatigue issues were reported by the subject. Moreover, stiffness control remained stable and no performance issues were experienced.

Future work will consist in extending the presented experiments by: *i)* Directly measuring human joint kinematic profiles (e.g. using IMUs or a stereophotogrammetric system) and comparing it with the ones estimated through forward kinematics equations which are affected by non-ideal human-robot coupling; *ii)* Measuring the muscular activity and compare it with free walking conditions; *iii)* Investigating user's adaptation to the action of the robot.

ACKNOWLEDGEMENT

This work was partially supported by the FP7 FET Proactive Initiative "Embodied Intelligence" of the European Commission, project no. ICT-2007.8.5-231451 - EVRYON (EVolving morphologies for human-Robot sYmbiotic interactiON). The work was also supported in part by the H133P0800007-NIDRR-ARRT fellowship. Thanks to Mr. Simone Galzerano and to Mr. Michelangelo Di Palo for their work on the mechanical design and thanks to Dr. Nicola Vitiello for the work on the control algorithms.

REFERENCES

[1] J. L. Pons, *Wearable Robots: Biomechatronic Exoskeletons*. John Wiley & Sons, Ltd, 2008.

[2] H. Herr, "Exoskeletons and orthoses: classification, design challenges and future directions," *J Neuroeng Rehabil*, vol. 6, no. 21, 2009.

[3] K. H. Low, "Robot-assisted gait rehabilitation: From exoskeletons to gait systems," in *Defense Science Research Conf and Expo (DSR)*, pp. 1–10, 2011.

[4] I. Díaz, J. J. Gil, and E. Sánchez, "Lower-limb robotic rehabilitation: Literature review and challenges," *J of Robotics*, 2011.

[5] E. Strickland, "Good-bye, wheelchair," *Spectrum, IEEE*, vol. 49, pp. 30–32, 2012.

[6] G. Zeilig, H. Weingarden, M. Zwecker, I. Dudkiewicz, A. Bloch, and A. Esquenazi, "Safety and tolerance of the Rewalk exoskeleton suit for ambulation by people with complete spinal cord injury: A pilot study," *J Spinal Cord Med*, vol. 35, no. 2, pp. 96–101, 2012.

[7] Rex bionics website, "http://rexbionics.com".

[8] Y. Sankai, "Hal: Hybrid assistive limb based on cybernics," in *Robotics Research* (M. Kaneko and Y. Nakamura, eds.), *Springer Tr Adv Robot*, vol. 66, pp. 25–34, Springer Berlin Heidelberg, 2011.

[9] R. Farris, H. Quintero, and M. Goldfarb, "Preliminary evaluation of a powered lower limb orthosis to aid walking in paraplegic individuals," *IEEE Trans Neural Syst Rehabil Eng*, 2011.

[10] P. D. Neuhaus, J. H. Noorden, T. J. Craig, T. Torres, J. Kirschbaum, and J. E. Pratt, "Design and evaluation of mina: A robotic orthosis for paraplegics," in *IEEE Int Conf Rehabil Robot (ICORR)*, pp. 1–8, 2011.

[11] S. Jezernik, G. Colombo, T. Keller, H. Frueh, and M. Morari, "Robotic orthosis lokomat: A rehabilitation and research tool," *Neuromodulation: Technology at the Neural Interface*, vol. 6, no. 2, pp. 108–115, 2003.

[12] J. Veneman, R. Kruidhof, E. Hekman, R. Ekkelenkamp, E. V. Asseldonk, and H. van der Kooij, "Design and evaluation of the LOPES exoskeleton robot for interactive gait rehabilitation," *IEEE Trans Neural Syst Rehabil Eng*, vol. 15, no. 3, pp. 379–386, 2007.

[13] Healthsouth website, "http://healthsouth.com".

[14] S. Banala, S. H. Kim, S. Agrawal, and J. Scholz, "Robot Assisted Gait Training With Active Leg Exoskeleton (ALEX)," *IEEE Trans Neural Syst Rehabil Eng*, vol. 17, no. 1, pp. 2–8, 2009.

[15] D. Aoyagi, W. Ichinose, S. Harkema, D. Reinkensmeyer, and J. Bobrow, "A robot and control algorithm that can synchronously assist in naturalistic motion during body-weight-supported gait training following neurologic injury," *IEEE Trans Neural Syst Rehabil Eng*, vol. 15, pp. 387–400, 2007.

[16] D. Accoto, N. L. Tagliamonte, G. Carpino, F. Sergi, M. Di Palo, and E. Guglielmelli, "pVEJ: A modular passive viscoelastic joint for assistive wearable robots," in *IEEE Int Conf Robot Autom (ICRA)*, pp. 3361–3366, 2012.

[17] N. L. Tagliamonte, F. Sergi, G. Carpino, D. Accoto, and E. Guglielmelli, "Design of a variable impedance differential actuator for wearable robotics applications," *Int Conf Int Rob Sys (IROS)*, pp. 2639–2644, 2010.

[18] N. L. Tagliamonte, F. Sergi, D. Accoto, G. Carpino, and E. Guglielmelli, "Double actuation architectures for rendering variable impedance in compliant robots: A review," *Mechatronics*, vol. 22, no. 8, pp. 1187–1203, 2012.

[19] A. Schiele and F. C. van der Helm, "Kinematic design to improve ergonomics in human machine interaction," *IEEE Trans Neural Syst Rehabil Eng*, vol. 14, pp. 456–69, 2006.

[20] N. Jarrassé, M. Tagliabue, J. V. G. Robertson, A. Maiza, V. Crocher, A. Roby-Brami, and G. Morel, "A methodology to quantify alterations in human upper limb movement during co-manipulation with an exoskeleton.," *IEEE Trans Neural Syst Rehabil Eng*, vol. 18, no. 4, pp. 389–97, 2010.

[21] F. Sergi, D. Accoto, N. Tagliamonte, G. Carpino, and E. Guglielmelli, "A systematic graph-based method for the kinematic synthesis of non-anthropomorphic wearable robots for the lower limbs," *Front Mech Eng*, vol. 6, pp. 61–70, 2011.

[22] F. Sergi, D. Accoto, N. Tagliamonte, G. Carpino, S. Galzerano, and E. Guglielmelli, "Kinematic synthesis, optimization and analysis of a non-anthropomorphic 2-DOFs wearable orthosis for gait assistance," in *Int Conf Int Rob Sys (IROS)*, pp. 4303–4308, 2012.

[23] G. Carpino, D. Accoto, F. Sergi, N. L. Tagliamonte, and E. Guglielmelli, "A novel compact torsional spring for series elastic actuators for assistive wearable robots," *J Mech Des*, vol. 134, no. 12, pp. 121002:1–10, 2012.

[24] H. Vallery, J. Veneman, E. van Asseldonk, R. Ekkelenkamp, M. Buss, and H. van der Kooij, "Compliant actuation of rehabilitation robots: benefits and limitations of series elastic actuators," *IEEE Robot Autom Mag*, vol. 15, no. 3, pp. 60–69, 2008.

[25] R. Ronsse, T. Lenzi, N. Vitiello, B. Koopman, E. van Asseldonk, S. M. M. De Rossi, J. van den Kieboom, et al. "Oscillator-based assistance of cyclical movements: model-based and model-free approaches," *Med Biol Eng Comput*, vol. 49, pp. 1173–1185, 2011.

[26] R. Pintelon and J. Schoukens, *System identification: a frequency domain approach*, IEEE Computer Society Press, 2001.

[27] D. Winter, *Biomechanics and Motor Control of Human Movement*, Wiley, 2009.

[28] F. Sergi, D. Accoto, G. Carpino, N. L. Tagliamonte, and E. Guglielmelli, "Design and characterization of a compact rotary series elastic actuator for knee assistance during overground walking," *Int Conf Biomed Robot Biomech (BioRob)*, 2012.